Concerted Use of Slab and Cluster Models in an ab Initio Study of Hydrogen Desorption from the Si(100) Surface†

J. A. Steckel, T. Phung,‡ and K. D. Jordan*

Department of Chemistry and Center for Molecular and Materials Simulations, University of Pittsburgh, Pittsburgh, Pennsylvania 15260

P. Nachtigall

J. Heyrovský Institute of Physical Chemistry, Academy of Sciences of the Czech Republic and Center for Complex Molecular Systems and Biomolecules, Dolejškova 3, 182 23 Prague 8, Czech Republic

Received: September 27, 2000; In Final Form: December 29, 2000

Slab and cluster models are used to study H_2 desorption from a single dimer of the Si(100)−2 × 1 surface. The cluster models are constructed using geometries obtained from slab-model optimizations. The largest cluster model considered, $Si_{89}H_{62}$, contains eight surface dimers and gives reaction and activation energies for desorption nearly identical with the slab-model values when the same electronic structure method is used. The barrier for H_2 desorption, calculated using the $Si_{89}H_{62}$ cluster model and the Becke3LYP functional, is 64.3 kcal/mol. When this result is corrected for the effects of basis set expansion and vibrational zero-point energy correction, the barrier decreases to about 61.0 kcal/mol, which is only 4.0 kcal/mol greater than the observed desorption barrier.

I. Introduction

A cut through bulk silicon along the 100 plane leaves each surface Si atom with two dangling bonds. The resulting surface undergoes a reconstruction to a (2 × 1) phase, consisting of parallel rows of Si−Si "dimers".[1,2] The lowering of the surface energy due to the creation of the Si−Si bond is offset by bond length distortions and the introduction of strain that may extend downward as much as five layers.[3] This leaves one dangling bond per surface atom, and hence, the reconstructed surface remains quite reactive. Interactions between the dangling bonds on a dimer impart partial π-bond character to the Si−Si bonds.[4−6] The π-bond strength has been calculated to be 5−12 kcal/mol for a symmetric dimer.[6] There is considerable evidence, both theoretical and experimental, that the bare dimers buckle with respect to the 100 plane.[7−11] As a dimer tilts, the lower Si atom moves almost into the plane of its three neighbors, essentially rehybridizing its four sp^3 orbitals into three occupied sp^2 orbitals and one unoccupied p orbital.[7,8] This necessarily reduces the π character of the dimer. The tilting of the buckled dimers is accompanied by lateral shifts and significant relaxation in subsurface Si atoms. The stabilization due to buckling has been calculated to be about 2 kcal/mol per surface dimer.[10] Several different buckling patterns are possible with the most stable believed to be the c(4 × 2) arrangement,[11] in which the direction of buckling alternates from dimer to dimer along a row and the buckling of dimers in adjacent rows is "out of phase". The symmetric dimer reconstruction as well as the (2 × 1), p(2 × 2), and c(4 × 2) phases is depicted in Figure 1.

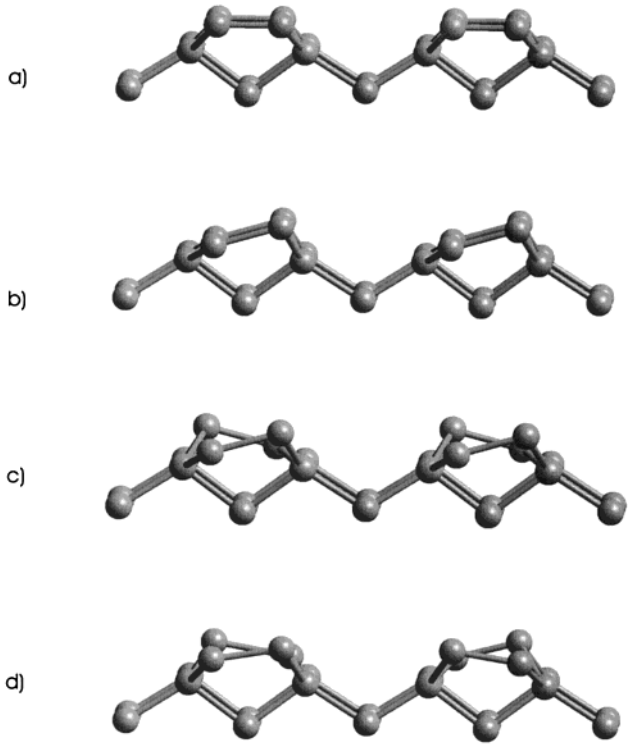

Figure 1. Si(100) surface reconstructions.

The Si(100) surface plays a critical role in the semiconductor industry, and despite intense theoretical and experimental study, questions about its fundamental surface chemistry remain unsettled.[6,8,12−42] Reactions of hydrogen with the Si(100) surface are particularly important as the formation of hydrides can be used to passivate the surface by tying up the dangling bonds. Moreover, hydrogen is often present during growth of the surface by chemical vapor deposition.[43] Hydrogen atom coverage of one monolayer leads to the Si(100)−2 × 1 monohydride structure in which each surface Si atom is bonded to one H

† Part of the special issue "John T. Yates, Jr., Festschrift".

‡ Present address: Department of Chemistry, Whittier College, Whittier, CA 90608.

10.1021/jp0035176 CCC: $20.00
Published on Web 02/22/2001

atom and the surface dimers remain intact. The dimers on the monohydride surface, in contrast to those on the bare Si(100) surface, are unbuckled in the minimum energy structure.[5,44] Complete saturation gives the Si(100)−1 × 1 dihydride surface with two H atoms per surface Si atom and leads to the disappearance of all Si surface dimers. Intermediate between the monohydride and the 1 × 1 dihydride is the Si(100)−3 × 1 hydride surface with alternating monohydride and dihydride structures.

A major impetus for modern studies of the adsorption of H_2 on and desorption of H_2 from the Si(100) surface was the pioneering work by Janda, Yates, and co-workers that showed, surprisingly, that H_2 desorption at submonolayer coverages follows first-order kinetics.[12,15] Subsequent studies showed that although the sticking probability of H_2 on this surface is small, desorbed H_2 molecules are vibrationally cold.[17,29] The former result implies a large barrier to adsorption, whereas the latter result would seem to indicate that the barrier to adsorption is low. Several mechanisms have been proposed to explain these results, including phonon-assisted sticking,[8,25−28] the involvement of defect sites,[18−22] and the existence of competitive pathways.[40,41]

One of the main difficulties in establishing, by means of computational studies, the mechanism of H_2 desorption/adsorption, and indeed of surface reactions in general, derives from uncertainties concerning the reliability of the theoretical methods used. Traditionally, two different approaches—cluster models and slab models—have been employed for modeling surface reactions. Both approaches have been used to study the Si(100)/H_2 system, and not surprisingly, considerable debate has ensued concerning the relative merits of these two approaches as applied to this problem.[31−36]

In the present work, we explore how cluster and slab models may be used in concert to mitigate the weaknesses inherent in each method when used alone. Specifically, we use structures from optimized slab models to generate cluster models. This allows us to use geometries that more realistically model the surface while permitting the use of theoretical methods that would not be feasible with the slab models. We use this approach to calculate the reaction energy and activation energy for H_2 desorption from a dimer site on the Si(100)−2 × 1 surface via the prepairing mechanism.[14] The goal of this study is to monitor the convergence of these energies with increasing slab-model and cluster-model size, rather than to establish the specific mechanism for H_2 desorption from and H_2 adsorption on the Si(100) surface. This work represents an extension of earlier studies of Nachtigall et al.[20,35] and Penev et al.[33] However, the present study goes beyond these earlier works in that larger slab and cluster models are considered.

II. Overview of Computational Methods

Before describing the details of our calculations, we first present a brief overview of slab-model and cluster-model approaches to modeling surface processes, emphasizing the main advantages and disadvantages inherent in each method.

A. Slab Models. In a slab model, an appropriate supercell is selected and replicated by use of periodic boundary conditions. When used with periodic basis functions (e.g., plane waves), the replication is done in three dimensions and a vacuum layer is introduced to isolate the top of one slab from the bottom of the next slab. With codes using localized basis sets, the replication perpendicular to the surface is not necessary. In carrying out such calculations, the researcher must decide on the size of the slab model including the vacuum layer, if required, how to terminate the dangling bonds on the bottom surface, and whether to freeze atoms in one or more layers of the slab. In addition, an appropriate level of electronic structure theory must be adopted.

Several supercells for studying H_2 desorption from the Si(100) surface are shown in Figure 2. Each supercell includes five layers of silicon atoms, and has the dangling bonds on the bottom layer of Si atoms terminated with H atoms. In applying such supercells to the H_2 adsorption/desorption problem, it is usual to freeze the positions of the bottom layers of Si atoms at their bulk positions and also to freeze the positions of the terminating H atoms. With respect to the description of the surface, the smallest cell, **a**, which repeats a single dimer, enforces 2 × 1 periodicity on the surface. The next two larger cells, **b** and **c**, treat, respectively, two and three dimers in the same row. Supercell **d** has four surface dimers, two in each of two adjacent rows. Supercell **e** has eight surface dimers, four in each of two adjacent rows.

Slab models, because of their use of periodic boundary conditions, eliminate some of the problems associated with edge effects. However, if the supercell is too small, there may be sizable errors in modeling low-coverage processes due to the interactions between adsorbed species in nearby cells. For example, with supercell **a**, H_2 desorption would occur simultaneously from all dimers on the surface, which would obviously introduce errors in the structures and in the reaction and activation energies. Supercells **b** and **c** are more realistic in that they introduce a degree of isolation between the dimers on which desorption is occurring. However, this isolation is only along the direction of the dimer row. Supercells **d** and **e** are preferable in that they isolate the desorption event both along and between rows.

If surface buckling is deemed to be important in the process under consideration, further restrictions are imposed on the choice of supercell. For example, periodic repetition of supercell **a** would not allow alternating buckling from dimer to dimer along a row. Model **b** is the smallest supercell that allows for treating an alternating buckling pattern along a row and allows for an alternating pattern of relaxation of subsurface Si atoms. On the other hand, the still larger supercell **c**, with three dimers in a row, cannot be used for representing the long-range alternating buckling pattern. Supercell **d** is the smallest that can be used to model the c(4 × 2) buckling pattern. Supercells **a** and **b** have been employed in several slab-model studies of the desorption of H_2 from the Si(100)−2 × 1/H surface.[8,25,27,30,33] Moreover, in their study of this process, Vittadini and Selloni used a supercell similar to **e**, but containing six layers instead of five.[31]

In addition to errors that may be introduced due to use of too small a supercell, there are the errors inherent in the use of approximate electronic structure methods. A particularly serious limitation is that accurate wave function based methods such as coupled cluster theory are unavailable with periodic codes. This, in turn, makes it difficult, using slab models alone, to obtain reliable estimates of the uncertainties in the calculated energy differences. Essentially all slab-model calculations on the Si(100)/ H_2 system, including our own, have been carried out using density functional theory (DFT) and plane-wave basis sets.[8,10,25,27,30,31,33,41] In current periodic DFT implementations, the available functionals, such as the Perdew−Wang 1991 (PW91)[46] and Becke−Perdue (BP)[47] functionals, do not include a portion of the exact exchange. Hybrid functionals such as Becke3LYP,[47] which include a portion of the exact exchange and have proven to be quite effective for nonperiodic applica-

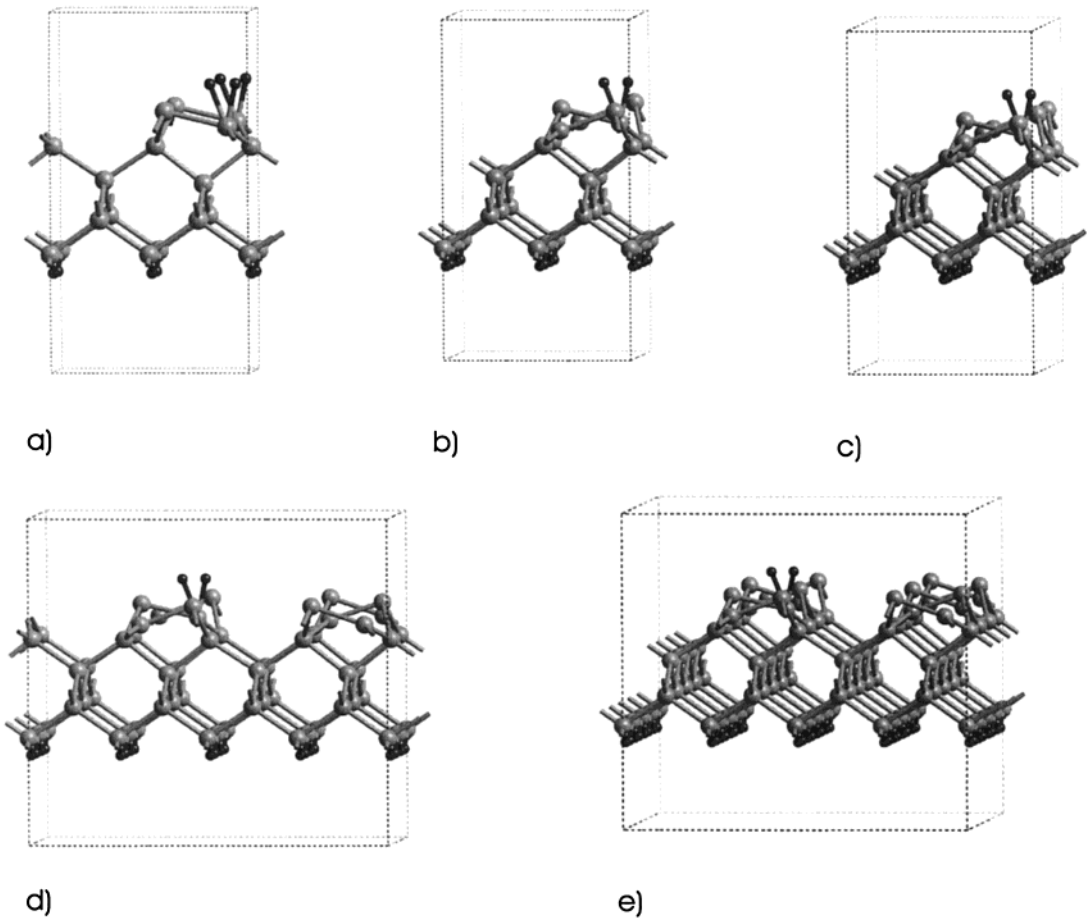

Figure 2. Examples of supercells for slab-model study of H_2 desorption from Si(100). Atoms that are intersected by the periodically repeated supercell appear more than once.

tions,[35,48] are not available. This is a drawback, since, as shown by Nachtigall et al.,[35] the Becke3LYP functional is more reliable for calculating the activation barrier for H_2 desorption from small cluster models than are the PW91 or BP functionals, which underestimate the barrier by about 10 kcal/mol.

B. Cluster Models. Cluster models have been extensively used for theoretical studies of reactions on surfaces.[6,12,18−23,32,33,35,38,42] The two major advantages of cluster models over slab models are (1) they can be used in conjunction with hybrid DFT methods and with wave function methods that treat high-order correlation effects, provided the cluster is not too large, and (2) they permit surface reactions to be studied at vanishingly small coverage. However, in using clusters to model surface reactions, one is presented with the issues of how to determine appropriate geometries and how to deal with subsurface dangling bonds. In addition, there is the question of whether the finite size of the cluster modifies the electronic structure to such an extent that the energy differences of interest are significantly affected.

The most common approach to dealing with the subsurface dangling bonds is to terminate them with H atoms.[6,12,18,36] Since H and Si atoms have similar electronegativities, this is not too drastic an approximation. Obtaining appropriate geometries has proven more problematical. For small cluster models, unconstrained geometry optimizations are unlikely to result in structures that accurately represent the surface process being modeled. For this reason, constrained optimizations have often been used when employing cluster models.[6,18,21,23,38] However, the optimal constraint procedure is unknown, and there is the possibility that the constrained optimizations do not adequately allow for geometry distortions during the course of a surface reaction. An alternative approach, employed by Penev et al.,[33] is to construct the cluster models by cutting out geometries from optimized slab models and terminating the subsurface dangling bonds with H atoms. However, these authors carried out partial geometry optimizations on the resulting cluster models, which makes this approach susceptible to the problems discussed above. In the present work we employ single-point energy calculations on cluster models generated from slab-models and without subsequent geometry reoptimization. Large slab models are used for generating the cluster models, and the convergence of the reaction and activation energies over a large range of cluster sizes is monitored.

III. Calculations

A. Slab Models. For our slab-model calculations, we used the Vienna Ab Initio Simulations Package (VASP)[49−52] and the PW91 exchange-correlation functional. Three slab models, **b**, **d**, and **e**, depicted above and containing, respectively, 20, 40, and 80 Si atoms per supercell, were employed. Use of such a large supercell is important for establishing convergence with respect to supercell size and for constructing more realistic cluster models. Each supercell contained five layers of Si atoms, with the two lowest layers being fixed at bulk positions. (We also carried out calculations in which the top four layers of Si atoms were allowed to relax, but these gave reaction and activation energies nearly identical with those obtained from the calculations in which only three layers were relaxed.) The positions of the H atoms terminating the bottommost silicon

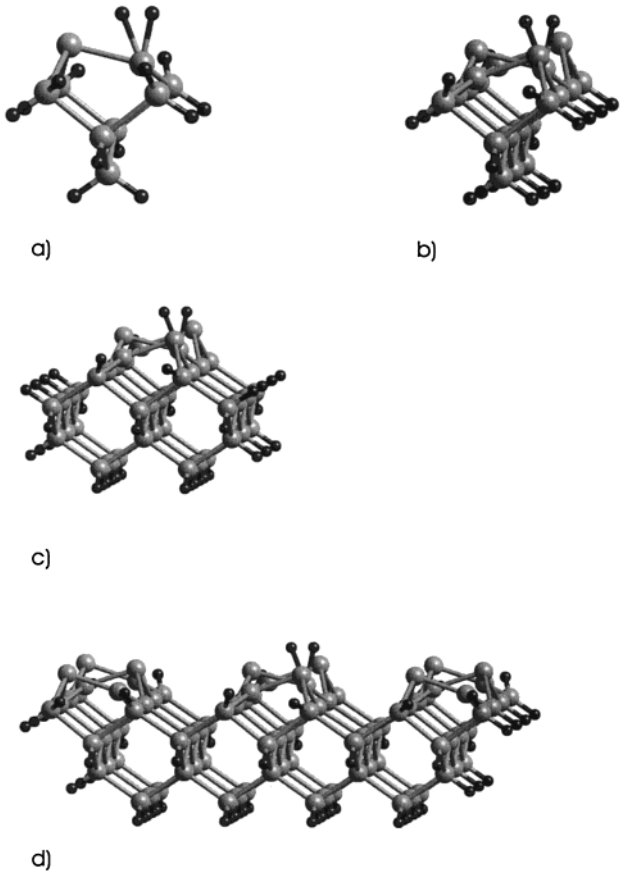

Figure 3. Cluster models used in the current work. All cluster models were generated from slab-model **e** geometries.

layer were also fixed. A vacuum layer of at least 7 Å was used to separate adjacent slabs. Reducing the vacuum layer by 1 Å caused changes of less than 0.1 kcal/mol in the activation and reaction energies. Test calculations were run using various plane-wave energy cutoffs and numbers of *k* points. Our final calculations used a plane-wave cutoff of 200 eV and two *k* points, for which we estimate the energy differences to be converged to 0.05 eV. This low an energy cutoff was made feasible by use of ultrasoft (Vanderbilt-type) pseudopotentials incorporated in the VASP program.[53]

Reactant and product geometries were optimized using the RMM-DIIS algorithm[54,55] until the forces on all movable ions were less than 0.10 eV/Å. The minimum energy path between the reactant and product, assuming the prepairing mechanism, was optimized by means of the nudged elastic band (NEB) algorithm,[56] in which the continuous reaction path is replaced with a set of discrete images. In our calculations, 16 images were used between the reactant and the product. The NEB optimizations were run until the forces on movable atoms in all images were less than 0.17 eV/Å. The energies of the images along the reaction path were fit to a spline curve and the maximum along the curve was associated with the transition state. The geometry of the transition state was determined by interpolation between the two images closest to the maximum.

B. Cluster Models. The four cluster models considered in the present study are depicted in Figure 3. The smallest cluster, Si_9H_{14}, has a single surface dimer, while the intermediate sized $Si_{21}H_{22}$ and $Si_{41}H_{38}$ cluster models both have three surface dimers along a single row. The latter two models differ in the numbers of subsurface Si atoms and associated terminating H atoms. Finally, the $Si_{89}H_{62}$ cluster model has nine dimers (three rows of three) in the surface. In the three larger cluster models,

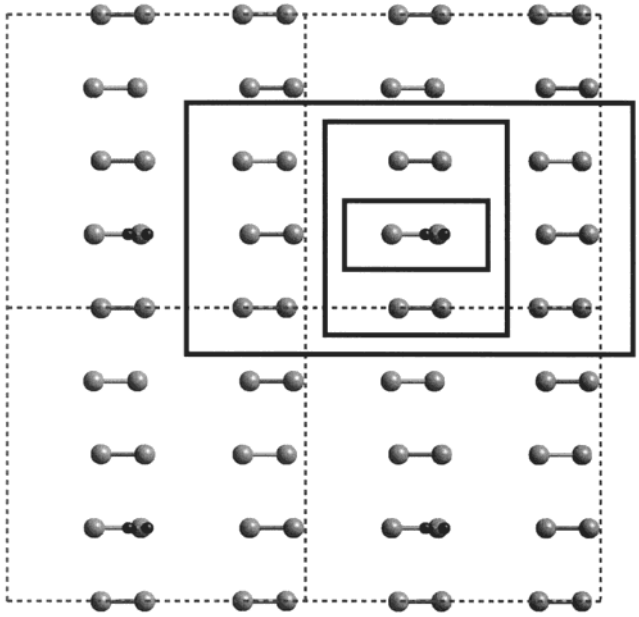

Figure 4. Relationship between the surface dimers in supercell **e** and the cluster models generated from it. The smallest box indicates the extent of the Si_9H_{14} cluster model, the next largest box indicates that of the $Si_{21}H_{22}$ and $Si_{41}H_{38}$ cluster models, and the largest box indicates the extent of the $Si_{89}H_{62}$ cluster model.

the chemisorbed hydrogens are located on the middle dimer. $Si_{89}H_{62}$ is the largest cluster used to date for studying H_2 desorption from the Si(100)-2×1 surface.

The positions of the Si atoms and the desorbing H atoms in each of the cluster models were taken from the slab-model calculations employing the 80 Si atom supercell **e**. For each cluster model, three different geometrical structures were considered: the reactant, which has a single monohydride site; the transition state; and the product, which consists of the bare Si(100)-2×1 surface plus H_2. The relation between the surface dimers in the cluster models and the slab model used in their generation is illustrated in Figure 4. The angles and dihedral angles involving the subsurface terminating H atoms were taken to be the same as the corresponding Si$-$Si$-$Si angles and Si$-$Si$-$Si$-$Si dihedral angles in the slab model. The bond lengths of the terminating Si$-$H bonds were taken to be 1.35 Å.[57]

For each cluster model, DFT calculations with the PW91 and Becke3LYP functionals were performed using the Gaussian 98 electronic structure program.[58] These calculations were done at an all-electron level and employed contracted Gaussian-type orbital basis sets. For all four cluster models, calculations were carried out using a 6-311G(d,p)[59,60] description of the Si atoms in the top two layers, the chemisorbed H atoms, and the uppermost terminating H atoms, a 6-31G(d)[61−63] description of the Si atoms in the third layer, and a 3-21G[64−69] description of the Si atoms in the lower layers and subsurface terminating H atoms. For the Si_9H_{14}, $Si_{21}H_{22}$, and $Si_{41}H_{38}$ clusters, calculations were also carried out with a more flexible basis set, with a 6-311G(2d,2p) description of the top layers, the chemisorbed H atoms, and the uppermost terminating H atoms, a 6-31G(d)[70] description of the Si atoms in the middle layer, and a 3-21G[71−74] description of the bottommost Si atoms and subsurface terminating H atoms.

In the case of the Si_9H_{14} cluster, MP2 and coupled cluster CCSD(T) calculations were also carried out to aid in estimating the errors in the energy differences from the DFT calculations. Finally, to estimate the vibrational zero-point energy corrections, full geometry optimizations were carried out on the $Si_{21}H_{22}$

TABLE 1: Reaction and Activation Energies and Geometrical Parameters from the Slab-Model Calculations[a]

slab model	energy differences: activation energy (kcal/mol)	energy differences: reaction energy (kcal/mol)		geometrical parameters[b]: H_1–H_2 (Å)	Si_1–H_1 (Å)	Si_1–H_2 (Å)	Si_1–Si_2 (Å)	α (deg)
2 dimers	52.6	42.2	reactant	3.473	1.501		2.411	0.5
			TS	1.015	1.712	1.800	2.465	12.6
			product	0.756			2.389	19.1
4 dimers		43.0	reactant	3.485	1.500		2.416	0.9
			product	0.771			2.398	18.7
8 dimers	53.4	43.0	reactant	3.474	1.501		2.413	0.9
			TS	0.980	1.702	1.777	2.466	14.0
			product	0.751			2.388	19.1

[a] These results were obtained using the Perdew−Wang 91 exchange-correlation functional. [b] H_1 and H_2 denote the desorbing H atoms, and Si_1 and Si_2 denote the Si atoms of the surface dimer involved in desorption. α gives the angle of the surface dimer with respect to the plane of the frozen layer of Si atoms.

cluster model using the Becke3LYP functional and a basis set employing a 6-31G(d,p) description of the six Si atoms in the top layer and the desorbing H atoms and a 3-21G description of all other atoms. Single-point energy calculations using the 6-311G(d,p)/6-31G(d)/3-21G basis set described above and both the Becke3LYP and PW91 functionals were performed on the optimized structures in order to gain insight into the magnitude of the errors that are introduced when using full geometry optimizations in conjunction with the $Si_{21}H_{22}$ cluster model.

IV. Results and Discussion

A. Slab-Model Results. The reaction and activation energies and geometrical parameters obtained from DFT calculations using the PW91 functional and slab models **b**, **d**, and **e** are summarized in Table 1. The activation energy and geometrical parameters for the transition state are not reported for the intermediate sized slab model **d** because the NEB reaction path optimizations were not sufficiently converged in this case. The reaction and the activation energies are seen to increase only slightly (i.e., by ≤0.8 kcal/mol) along the sequence of supercells **b**, **d**, and **e**.

The geometrical parameters obtained for the three supercells are also similar. These results indicate that even the smallest supercell **b** is appropriate for studying H_2 desorption via the prepairing mechanism. With the supercell model **e**, our PW91 calculations give reaction and activation energies for H_2 desorption of 43.0 and 53.4 kcal/mol, respectively, slightly lower than the values reported in previous studies employing slab models with smaller supercells and the PW91 functional.[8,30,31,33]

B. Cluster-Model Results. The reaction and activation energies obtained using the Becke3LYP and PW91 functionals and the Si_9H_{14}, $Si_{21}H_{22}$, $Si_{41}H_{38}$, and $Si_{89}H_{62}$ cluster models described above are summarized in Table 2. We consider first the results obtained with the 6-311G(d,p)/6-31G(d)/3-21G basis set. For both functionals, both the reaction and activation energies decrease by about 10 kcal/mol in going from the Si_9H_{14} to the $Si_{21}H_{22}$ cluster, but decrease by less than 1.8 kcal/mol in progressing to the $Si_{41}H_{38}$ cluster and by less than 0.8 kcal/mol in going from the $Si_{41}H_{38}$ to the $Si_{89}H_{62}$ cluster model. For the PW91 functional, the results obtained for the $Si_{89}H_{62}$ cluster model are in close agreement with those from the slab-model calculations (with discrepancies between the two sets of activation and reaction energies being 0.5 and 1.8 kcal/mol, respectively). It is clear from these results that the frequently used Si_9H_{14} cluster is inadequate for accurately describing H_2 desorption from the Si(100)−2 × 1 surface. On the other hand, the cluster models containing only three surface dimers, (i.e., $Si_{21}H_{22}$ and $Si_{41}H_{38}$), represent a dramatic improvement over the Si_9H_{14} cluster for describing the H_2 desorption process.

TABLE 2: Reaction and Activation Energies from Single-Point Cluster-Model Calculations[a]

cluster model	activation energy (kcal/mol): B3LYP	activation energy (kcal/mol): PW91	reaction energy (kcal/mol): B3LYP	reaction energy (kcal/mol): PW91
Si_9H_{14}	76.1	66.6	64.1	57.7
	(74.7)	(65.0)	(61.9)	(55.6)
$Si_{21}H_{22}$	66.5	56.5	53.6	47.3
	(65.5)	(55.6)	(51.8)	(45.5)
$Si_{41}H_{38}$	65.1	54.7	51.8	45.2
	(64.3)	(53.8)	(50.5)	(43.9)
$Si_{89}H_{62}$	64.3	53.9	51.6	44.8
	(63.5)[b]	(53.0)[b]	(50.3)[b]	(43.5)[b]

[a] Results obtained using the mixed 6-311G(d,p)/6-31G(d)/3-21G basis set are reported first, and those obtained using the larger 6-311G(2d,2p)/6-31G(d)/3-21G basis set are reported underneath in parentheses. Vibrational zero-point energy corrections are not included in the results reported in the table. [b] For the $Si_{89}H_{62}$ cluster, the activation and reaction energies for the larger 6-311G(2d,2p)/6-31G(d)/3-21G basis set have been estimated by correcting the results obtained with the smaller 6-311G(d,p)/6-31G(d)/3-21G basis set with the energy changes found in going from the smaller to the larger basis set for the $Si_{41}H_{38}$ cluster.

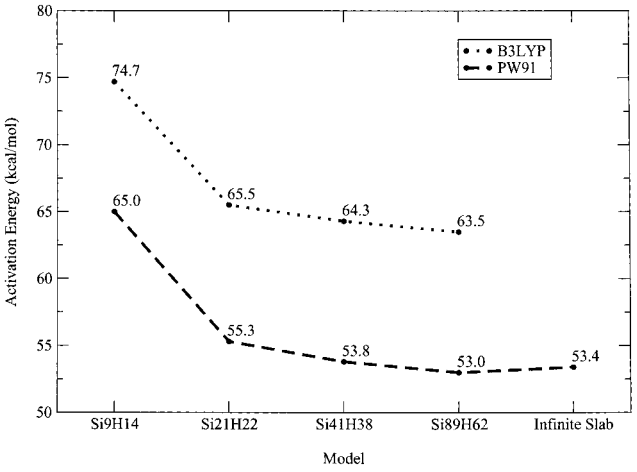

Figure 5. Activation energies obtained using the 6-311G(2d,2p)/6-31G(d)/3-21G basis set plotted as a function of cluster size. For the $Si_{89}H_{62}$ cluster, the activation energies for the 6-311G(2d,2p)/6-31G(d)/3-21G basis set were estimated as described in the text. The slab-model results are included for comparison.

Calculations with the larger 6-311G(2d,2p)/6-31G(d)/3-21G basis set were carried out only for the Si_9H_{14}, $Si_{21}H_{22}$, and $Si_{41}H_{38}$ cluster models. For the $Si_{41}H_{38}$ cluster model, this expansion of the basis set led to 0.9−1.3 kcal/mol reductions

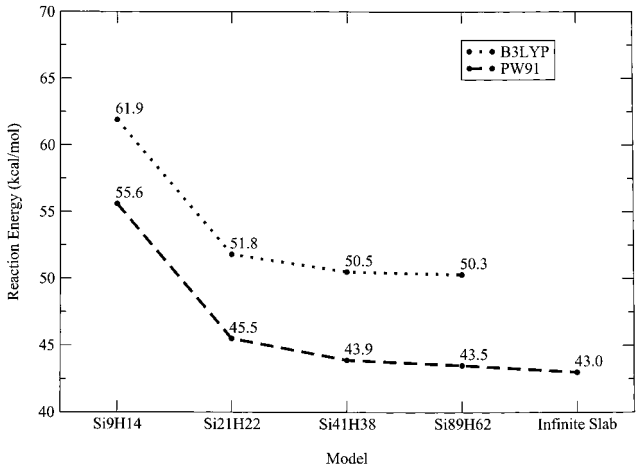

Figure 6. Reaction energies obtained using the 6-311G(2d,2p)/6-31G(d)/3-21G basis set plotted as a function of cluster size. For the $Si_{89}H_{62}$ cluster, the reaction energies for the 6-311G(2d,2p)/6-31G(d)/3-21G basis set were estimated as described in the text. The slab-model results are included for comparison.

TABLE 3: Comparison of DFT, MP2, and CCSD(T) Results for the Si_9H_{14} Cluster Model[a]

activation energy (kcal/mol)			reaction energy (kcal/mol)		
B3LYP	MP2	CCSD(T)	B3LYP	MP2	CCSD(T)
76.1 (74.7)	79.8 (74.7)	80.4 (75.3)[b]	64.1 (61.9)	65.8 (61.9)	65.2 (61.2)[b]

[a] Results obtained using the mixed 6-311G(d,p)/6-31G(d)/3-21G basis set are reported first, and those obtained using the larger 6-311G(2d,2p)/6-31G(d)/3-21G basis set are reported underneath in parentheses. Vibrational zero-point energy corrections are not included. [b] The CCSD(T) results with the larger 6-311G(2d,2p)/6-31G(d)/3-21G basis set have been estimated using a G2-like approach, as discussed in the text.

in the activation and reaction energies as calculated using the DFT methods. (The sensitivity to the basis set was slightly greater for the smaller clusters.) The energy changes accompanying the basis set expansion found for the $Si_{41}H_{38}$ cluster model were applied to the small basis set results for the $Si_{89}H_{62}$ cluster model. This brings the predictions of the activation and reaction energies obtained using the $Si_{89}H_{62}$ cluster model to within 0.5 kcal/mol of the slab-model results (again using the PW91 functional throughout). These estimated values are included in Table 2 and are also reported in Figures 5 and 6. Further expansion of the basis set is not expected to significantly impact the activation and reaction energies for H_2 desorption as calculated using density functional methods.

The reaction and activation energies calculated with the Becke3LYP functional are consistently higher by about 7 and 10 kcal/mol, respectively, than those calculated with the PW91 functional. This is consistent with the findings of Nachtigall et al. for small cluster models.[35] With the 6-311G(d,p)/6-31G(d)/3-21G basis set and the $Si_{89}H_{62}$ cluster model, the Becke3LYP calculations give an activation energy of 64.3 kcal/mol, about 7 kcal/mol higher than the measured value of 57 kcal/mol.[75,76] We estimate that in the complete basis set limit the Becke3LYP activation energy for hydrogen desorption from a dimer site on the Si(100) would be about 63.5 kcal/mol, 6 kcal/mol greater than the experimental value.

We now turn to a discussion of the errors inherent in the Becke3LYP method as applied to the H_2 desorption process. For the Si_9H_{14} cluster, the activation and reaction energies obtained using MP2 and CCSD(T) methods agree to within 1 kcal/mol, which indicates that, despite the biradical character of the bare Si−Si surface dimer, even the MP2 method provides a good description of H_2 desorption from the dimer site. Moreover, with the larger 6-311G(2d,2p)/6-31G(d)/3-21G basis set, the Becke3LYP results for the activation and reaction energies agree to within 0.6 kcal/mol of the CCSD(T) values. (See Table 3.) (CCSD(T) results for the larger basis set were estimated using a G2-like procedure,[77] namely by combining the CCSD(T) energies calculated using the smaller basis set and the differences in the MP2 energies calculated using the two basis sets.) We have also carried out MP2 calculations for the $Si_{21}H_{22}$ cluster model and here too find the MP2-level energy differences to be nearly identical with those obtained with the Becke3LYP method. In light of these results, we conclude that the Becke3LYP method is able to give quantitatively correct activation energies for H_2 desorption from dimer sites of the Si(100)−2 × 1 surface. Moreover, as noted above, calculations using the largest cluster model considered, $Si_{89}H_{62}$, give nearly the same results as found for large slab models. Thus, Becke3LYP calculations on the $Si_{89}H_{62}$ cluster model are expected to provide an accurate estimate of the activation energy for H_2 loss directly from a dimer site on the Si(100) surface.

It is necessary to consider also the contributions of vibrational zero-point energy (ZPE). For this purpose, we have performed full geometry optimizations using the Becke3LYP functional and the truncated 6-31G(d)/3-21G basis set on the $Si_{21}H_{22}$ cluster models and used the optimized structures to calculate the vibrational frequencies in the harmonic approximation. Using these frequencies, we find that the vibrational zero-point energy corrections act so as to decrease the activation and reaction energies by about 2.5 and 4.5 kcal/mol, respectively. Incorporating this correction, we obtain a value of 61.0 kcal/mol for our best estimate for the activation energy to desorb H_2 from a single dimer of the Si(100) surface.

The optimized $Si_{21}H_{22}$ cluster models were used in subsequent single-point DFT energy calculations using the 6-311G(d,p)/6-31G(d)/3-21G basis set. The geometrical parameters for the

TABLE 4: Results from Geometry Optimization of the $Si_{21}H_{22}$ Cluster Model

	B3LYP energy differences[a]			geometrical parameters[b]				
model	activation energy (kcal/mol)	reaction energy (kcal/mol)		H_1–H_2 (Å)	Si_1–H_1 (Å)	Si_1–H_2 (Å)	Si_1–Si_2 (Å)	α (deg)
$Si_{21}H_{22}$ cluster (from slab model)	66.5	53.6	reactant	3.474	1.501		2.413	0.9
			TS	0.980	1.702	1.777	2.466	14.0
			product	0.751			2.388	19.1
optimized $Si_{21}H_{22}$ cluster[c]	66.5	52.2	reactant	3.584	1.491		2.376	13.7
			TS	1.005	1.647	1.671	2.466	4.8
			product	0.743			2.304	10.3

[a] Energy differences are obtained via single-point B3LYP calculations using the mixed 6-311G(d,p)/6-31G(d)/3-21G basis set. [b] H_1 and H_2 denote the desorbing H atoms, Si_1 and Si_2 denote the Si atoms of the dimer from which they are desorbing, and α is the dimer angle. [c] The cluster models were optimized using the B3LYP functional and a mixed 6-31G(d)/3-21G basis set.

optimized structures as well as the associated activation and reaction energies are presented in Table 4. Most strikingly, the activation energy obtained using the fully relaxed cluster model is identical with that generated using the geometries cut out from the slab models. In addition, there is a difference of only 1.4 kcal/mol between the reaction energies calculated using the two sets of geometries. It follows, therefore, that the changes in the activation energy in going from the $Si_{21}H_{22}$ to the $Si_{89}H_{62}$ cluster model are primarily electronic in nature (rather than being due to how the cluster was terminated).

V. Conclusions

Slab models containing up to eight surface Si−Si dimers in the supercell have been used with periodic boundary conditions and the PW91 functional to study H_2 desorption from a surface dimer according to the prepairing mechanism. These calculations reveal the activation energy is already well converged in a slab model with only two surface dimers in the supercell. The largest slab model was used to construct a series of cluster models with one, three, and nine surface dimers. These were used to monitor the convergence of the activation and reaction energies for H_2 desorption with cluster size. It is shown that DFT calculations (using the PW91 functional) with the largest cluster model give nearly the same reaction and activation energies as obtained using the slab models. Moreover, these energy differences are already close to being converged in cluster models containing only three surface dimers.

The activation energies obtained with the Becke3LYP functional are consistently 10 kcal/mol higher than the PW91 values. Comparison with the results of MP2 and CCSD(T) calculations on the Si_9H_{14} cluster model leads us to conclude that the Becke3LYP functional is quite reliable for describing the activation energy for H_2 desorption from a surface dimer. For the $Si_{89}H_{62}$ cluster model, Becke3LYP calculations using the 6-311G(d,p)/6-31G/3-21G basis give an activation energy of 64.3 kcal/mol. This is reduced to 61.0 kcal/mol, which is only 4 kcal/mol greater than the measured activation energy for H_2 desorption from the Si(100) surface, when the effects of expansion of the basis set and of vibrational zero-point energy are included.

In addition to the errors in the activation energy due to the use of the $Si_{89}H_{62}$ cluster model (in place of the extended surface) and of the Becke3LYP/6-311G(2d,2p)/6-31G(d)/3-21G level of theory, which are believed to be individually less than 1 kcal/mol, there are other sources of error including the use of the PW91 functional for the geometry optimizations, discretization of the reaction path in the NEB calculations to obtain the optimized transition state geometries, and the use of vibrational frequencies from the $Si_{21}H_{22}$ cluster model to estimate the vibrational zero-point energies. In light of the errors inherent in the calculations, we conclude that our best estimate of the activation energy for H_2 desorption is consistent with the measured activation energy.

Several papers have pointed out that the dynamics associated with the H_2 adsorption/desorption process appears to be inconsistent with the prepairing mechanism.[21,26,27,34,37,38,41] One of the most recent papers addressing this issue provided evidence that two processes, the prepairing mechanism involving a single dimer site and a second process involving two adjacent dimer sites, are important in the H_2 adsorption/desorption process.[41]

The present study has shown that a combined slab- and cluster-model approach is well suited for obtaining accurate estimates of reaction and activation energies for surface processes. The application of this approach to the "two dimer" and other possible reaction pathways for the Si(100)/H_2 system would be valuable for providing a reliable, consistent set of data for subsequent kinetic Monte Carlo modeling of the kinetics.

Acknowledgment. We thank John Yates for many inspiring discussions of chemical reactions on semiconductor surfaces. We acknowledge a grant of computer time from NCSA. Part of the calculations were carried out on the IBM 43P computer cluster in the Center for Molecular and Materials Simulations, funded by the NSF and IBM. J.A.S. thanks the Lubrizol Corporation for fellowship support. T.P. was supported by a NSF REU grant to the University of Pittsburgh.

References and Notes

(1) Schlier, R. E.; Farnsworth, H. E. *J. Chem. Phys.* **1959**, *30*, 917.
(2) Tromp, R. M.; Hamers, R. J.; Demuth, J. E. *Phys. Rev. Lett.* **1985**, *55*, 1303.
(3) Appelbaum, J. A.; Hamann, D. R. *Surf. Sci.* **1978**, *74*, 21.
(4) Appelbaum, J. A.; Baraff, G. A.; Hamann, D. R. *Phys. Rev. B* **1976**, *14*, 588.
(5) Boland, J. J. *Phys. Rev. Lett.* **1991**, *67*, 1539.
(6) Nachtigall, P.; Jordan, K. D.; Janda, K. C. *J. Chem. Phys.* **1991**, *95*, 8652.
(7) Chadi, D. J. *Phys. Rev. Lett.* **1979**, *43*, 43.
(8) Pehlke, E.; Scheffler, M. *Phys. Rev. Lett.* **1995**, *74*, 952.
(9) Hamers, R. J.; Tromp, R. M.; Demuth, J. E. *Phys. Rev. B* **1986**, *34*, 5343.
(10) Dąbrowski, J.; Scheffler, M. *Appl. Surf. Sci.* **1992**, *56*−*58*, 15.
(11) (a) Yokoyama, T.; Takayanagi, K. *Phys. Rev B* **2000**, *61*, 5078. (b) Boguslawski, P.; Zhang, Q.-M.; Zhang, Z.; Bernholc, J. *Phys. Rev. Lett.* **1994**, *72*, 3694. (c) Northrup, J. E. *Phys. Rev. B* **1993**, *47*, 1002.
(12) Raghavachari, K. *J. Chem. Phys.* **1986**, *84*, 5672.
(13) Sinniah, K.; Sherman, M. G.; Lewis, L. B.; Weinberg, W. H.; Yates, J. T., Jr.; Janda, K. C. *Phys. Rev. Lett.* **1989**, *62*, 567.
(14) Wise, M. L.; Koehler, B. G.; Gupta, P.; Coon, P. A.; George, S. M. *Surf. Sci.* **1991**, *258*, 166.
(15) Sinniah, K.; Sherman, M. G.; Lewis, L. B.; Weinberg, W. H.; Yates, J. T., Jr.; Janda, K. C. *J. Chem. Phys.* **1990**, *92*, 5700.
(16) D'Evelyn, M. P.; Yang, Y. L.; Sutcu, L. F. *J. Chem. Phys.* **1992**, *96*, 852.
(17) Kolasinski, K. W.; Shane, S. F.; Zare, R. N. *J. Chem. Phys.* **1992**, *96*, 3995.
(18) Jing, Z.; Whitten, J. L. *J. Chem. Phys.* **1993**, *98*, 7466.
(19) Wu, C. J.; Ionova, I. V.; Carter, E. A. *Surf. Sci.* **1993**, *295*, 64.
(20) Nachtigall, P.; Jordan, K. D.; Sosa, C. *J. Chem. Phys.* **1994**, *101*, 8037.
(21) Radeke, M.; Carter, E. A. *Phys. Rev. B* **1996**, *54*, 11803.
(22) Radeke, M.; Carter, E. A. *Phys. Rev. B* **1997**, *55*, 4649.
(23) Nachtigall, P.; Jordan, K. D.; Sosa, C. *J. Phys. Chem.* **1993**, *97*, 11666.
(24) Brenig, W.; Gross, A.; Russ, B. *Z. Phys. B: Condens. Matter* **1994**, *96*, 231.
(25) Kratzer, P.; Hammer, B.; Nørskov, J. K. *Chem. Phys. Lett.* **1994**, *229*, 64.
(26) (a) Bratu, P.; Brenig, W.; Gross, A.; Hartmann, M.; Höfer, U.; Kratzer, P.; Russ, R. *Phys. Rev. B* **1996**, *54*, 5978. (b) Dürr, M.; Raschke, M. B.; Höfer, U. *J. Chem. Phys.* **1999**, *111*, 10411.
(27) Gross, A.; Bockstedte, M.; Scheffler, M. *Phys. Rev. Lett.* **1997**, *79*, 701.
(28) Hilf, M. F.; Brenig, W. *J. Chem. Phys.* **2000**, *112*, 3113.
(29) Kolasinski, K. W.; Nessler, W.; de Meijere, A.; Hasselbrink, E. *Phys. Rev. Lett.* **1994**, *72*, 1356.
(30) Kratzer, P.; Hammer, B.; Nørskov, J. K. *Phys. Rev. B* **1995**, *51*, 13432.
(31) Vittadini, A.; Selloni, A. *Chem. Phys. Lett.* **1995**, *235*, 334.
(32) Jing, Z.; Whitten, J. L. *J. Chem. Phys.* **1995**, *102*, 3867.
(33) Penev, E.; Kratzer, P.; Scheffler, M. *J. Chem. Phys.* **1999**, *110*, 3986.
(34) Luntz, A. C.; Kratzer, P. *J. Chem. Phys.* **1995**, *104*, 3075.
(35) Nachtigall, P.; Jordan, K. D.; Smith, A.; Jónsson, H. *J. Chem. Phys.* **1996**, *104*, 148.
(36) Doren, D. J. *Adv. Chem. Phys.* **1996**, *95*, 1.
(37) Kratzer, P.; Russ, R.; Brenig, W. *Surf. Sci.* **1996**, *345*, 125.
(38) Radeke, M.; Carter, E. A. *Surf. Sci.* **1996**, *355*, L292.
(39) Dürr, M.; Raschke, M.; Höfer, U. *J. Chem. Phys.* **1999**, *111*, 10411.
(40) Biedermann, A.; Knoesel, E.; Hu, Z.; Heinz, T. F. *Phys. Rev. Lett.* **1999**, *83*, 1810.
(41) Zimmerman, F. M.; Pan, X. *Phys. Rev. Lett.* **2000**, *85*, 618.

(42) Shoemaker, J.; Burggraf, L. W.; Gordon, M. S. *J. Chem. Phys.* **2000**, *112*, 2994.
(43) Boland, J. J. *Adv. Phys.* **1993**, *42*, 129 and references therein.
(44) Wang, Y.; Bronikowski, M. J.; Hamers, R. J. *Surf. Sci.* **1994**, *311*, 64.
(45) The PW91 functional (Perdew, J. P.; Chevary, J. A.; Vosko, S. H.; Jackson, K. A.; Pederson, M. R.; Singh, D. J.; Fiolhais, C. *Phys. Rev. B* **1992**, *46*, 6671) was developed by J. P. Perdew and Y. Wang (unpublished results).
(46) The BP functional combines Becke's 1988 exchange functional (Becke, A. D. *Phys. Rev. A* **1988**, *38*, 3098) with the 1986 correlation functional of Perdew (Perdew, J. P. *Phys. Rev. B* **1986**, *33*, 8822).
(47) Becke3LYP combines the three-parameter non local exchange functions of Becke (Becke, A. D. *Phys. Rev. A* **1993**, *98*, 5648) and the LYP correlational functional (Lee, C.; Yang, W.; Parr, R. G. *Phys. Rev. B* **1993**, *37*, 785).
(48) Hamprecht, F. A.; Cohen, A. J.; Tozer, D. J.; Handy, N. C. *J. Chem. Phys.* **1998**, *109*, 6264.
(49) Kresse, G.; Hafner, J. *Phys. Rev. B* **1993**, *47*, 558.
(50) Kresse, G.; Hafner, J. *Phys. Rev. B* **1994**, *49*, 14251 1994.
(51) Kresse, G.; Furthmüller, J. *Comput. Mat. Sci.* **1996**, *6*, 15.
(52) Kresse, G.; Furthmüller, J. *Phys. Rev. B* **1996**, *54*, 11169.
(53) (a) Vanderbilt, D. *Phys. Rev. B* **1990**, *41*, 7892. (b) Kresse, G.; Hafner, J. *J. Phys.*: *Condens. Matter* **1994**, *6*, 8245.
(54) Pulay, P. *Chem. Phys. Lett.* **1980**, *73*, 393.
(55) Wood, D. M.; Zunger, A. *J. Phys. A* **1985**, 1343.
(56) Mills, G.; Jónsson, H.; Schenter, G. K. *Surf. Sci.* **1995**, 324, 305.
(57) An Si−H bond length of 1.35 Å for terminating hydrogens was assumed for the sake of consistency with the slab models, on which the bottommost layer terminating Si−H bond lengths were optimized. Changing the Si−H bond lengths of the terminating H atoms to a more typical value of 1.5 Å proved relatively unimportant for the reaction and activation energies, introducing changes of less than 0.4 kcal/mol for the Si_9H_{14} and $Si_{21}H_{22}$ models and 0.1 kcal/mol for the $Si_{41}H_{38}$ model.
(58) Frisch, M. J.; et al. *Gaussian 98*, Revision A.9; Gaussian, Inc.: Pittsburgh, PA, 1998.
(59) McLean, A. D.; Chandler, G. S. *J. Chem. Phys*. **1980**, *72*, 5639.
(60) Krishnan, R.; Binkley, J. S.; Seeger, R.; Pople, J. A. *J. Chem. Phys.* **1980**, *72*, 650.
(61) Hehre, W. J.; Ditchfield, R.; Pople, J. A. *J. Chem. Phys.* **1972**, *56*, 2257.
(62) Gordon, M. S. *Chem. Phys. Lett.* **1980**, *76*, 163.
(63) Hariharan, P. C.; Pople, J. A. *Theor. Chim. Acta* **1973**, *28*, 213.
(64) Binkley, J. S.; Pople, J. A.; Hehre, W. J. *J. Am. Chem. Soc.* **1980**, *102*, 939.
(65) Gordon, M. S.; Binkley, J. S.; Pople, J. A.; Pietro, W. J.; Hehre, W. J. *J. Am. Chem. Soc.* **1982**, *104*, 2797.
(66) Pietro, W. J.; Francl, M. M.; Hehre, W. J.; Defrees, D. J.; Pople, J. A.; Binkley, J. S. *J. Am. Chem. Soc.* **1982**, *104*, 5039.
(67) Dobbs, K. D.; Hehre, W. J. *J. Comput. Chem*. **1986**, 7, 359.
(68) Dobbs, K. D.; Hehre, W. J. *J. Comput. Chem*. **1987**, *8*, 861.
(69) Dobbs, K. D.; Hehre, W. J. *J. Comput. Chem.* **1987**, *8*, 880.
(70) Gordon, M. S. *Chem. Phys. Lett.* **1980**, *76*, 163.
(71) Gordon, M. S.; Binkley, J. S.; Pople, J. A.; Pietro W. J.; Hehre, W. J. *J. Am. Chem. Soc.* **1982**, *104*, 2797.
(72) Pietro, W. J.; Francl, M. M.; Hehre, W. J.; Defrees, D. J.; Pople, J. A.; Binkley, J. S. *J. Am. Chem. Soc.* **1982**, *104*, 5039.
(73) Dobbs, K. D.; Hehre, W. J. *J. Comput. Chem*. **1986**, 7, 359.
(74) Dobbs, K. D.; Hehre, W. J. *J. Comput. Chem*. **1987**, *8*, 861.
(75) Flowers, M. C.; Jonathan, N. B. H.; Liu, Y.; Morris, A. *J. Chem. Phys.* **1993**, *99*, 7038.
(76) Höfer, U.; Li, L.; Heinz, T. F. *Phys. Rev. B* **1992**, *45*, 9485.
(77) Curtiss, L. A.; Raghavachari, K.; Pople, J. A. *J. Chem. Phys.* **1993**, *98*, 1293.